Editors' Suggestion

Interaction of degenerate higher-order modes in periodic superconducting rf accelerating structures

V. Yakovlev,* S. Belomestnykh, T. Khabiboulline, and A. Lunin
Fermi National Accelerator Laboratory (FNAL), Kirk and Pine St., Batavia, Illinois 60510, USA

(Received 20 July 2026; accepted 27 October 2026; published 17 November 2026)

Some higher-order mode (HOM) passbands in multicell superconducting rf accelerating structures may become "flat," meaning that they have an extremely narrow bandwidth due to weak coupling between cells. In the presence of random perturbations caused by mechanical imperfections of the cell shapes, such passbands can split into individual cell resonances that are weakly coupled or completely uncoupled from the beam pipes. As a result, these modes can exhibit high-quality factors and large R/Q values, potentially leading to beam instabilities, emittance growth, and excessive cryogenic losses. This effect was observed in a high-beta five-cell 650 MHz (HB650) prototype cavity developed for the PIP-II project. An analytical theory explaining the origin of this phenomenon, along with methods to mitigate it, is presented in this paper. The HB650 cavity was successfully redesigned to eliminate the flat HOM passband and prevent the associated detrimental effects.

DOI: 10.1103/blpm-g4sl

I. INTRODUCTION

The excitation of higher-order modes (HOMs) in superconducting rf (SRF) cavities is a well-known phenomenon that is routinely considered during cavity design. HOMs with highly loaded quality factors and large R/Q values can be excited by the accelerated beam to significant amplitudes, potentially resulting in beam emittance dilution, excessive cryogenic load, and even beam instabilities. Particular attention must be paid to the so-called trapped modes; see, for example, Ref. [1]. These modes are characterized by electromagnetic fields concentrated in the central cells of a multicell cavity, with weak field amplitudes at the ends, resulting in highly loaded quality factors and large R/Q values.

The excitation of HOMs has been extensively studied and is generally well understood. Dedicated conferences and numerous publications are devoted to this subject, and at first glance, it may appear difficult to identify any new effects. However, during the development of the high-beta, five-cell 650 MHz SRF cavity prototype [2] for the PIP-II project [3], an unexpected phenomenon was encountered. In real cavities with mechanical imperfections, instead of the predicted fifth monopole HOM passband, a set of individual cell resonances with closely spaced frequencies around 1988 MHz was observed [4].

The cavity layout and the results of axial field distribution measurements using the bead-pull technique are shown in Fig. 1, which demonstrates the presence of trapped monopole modes. Individual resonances localized in the central cells of the cavity are weakly coupled to the input coupler and, therefore, exhibit very highly loaded quality factors. Since the electromagnetic fields of these resonances are predominantly confined within individual cells, the fields on the axis are also highly localized, resulting in a high transit time factor and, consequently, large R/Q values. Combined with a highly loaded quality factor, this leads to a large shunt impedance.

Results of simulations for an ideal cavity [5] show an extremely narrow passband with a bandwidth of approximately 40 kHz. The weak coupling between the cavity cells is caused by the small electric and magnetic fields in the vicinity of the cavity apertures. The corresponding electric field patterns in the cavity are shown in Fig. 2 (left). Due to weak coupling between the cells, even slight geometry perturbations of ± 0.2 mm rms can cause the passband to split into individual cell resonances [5], as shown in Fig. 2 (right).

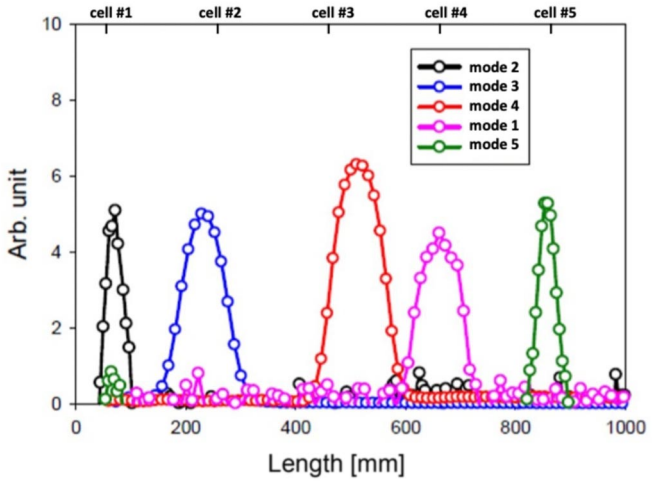
Attempts to increase the intercell coupling coefficient K_c by enlarging the cavity aperture from the initial value of 50 mm to 60 mm did not significantly improve the situation. The coupling coefficient remains relatively insensitive to the aperture size until a certain critical value is reached. However, by combining the aperture increase with an increase in the cell length, i.e., increasing the cavity geometric beta β_G from 0.9 to 0.92, it was possible to increase the intercell coupling coefficient to an

*Contact author: yakovlev@fnal.gov

Published by the American Physical Society under the terms of the Creative Commons Attribution 4.0 International license. Further distribution of this work must maintain attribution to the author(s) and the published article's title, journal citation, and DOI.



(a)



(b)

FIG. 1. (a) Photograph of the high-beta, five-cell 650 MHz SRF cavity prototype developed for the PIP-II project, with the input coupler port located on the left-hand side, and (b) bead-pull measurements of the on-axis field profiles for five monopole modes, showing excellent agreement with the prediction that, in a real cavity with random variations in cell geometries, the passband splits into individual cell resonances.

acceptable level and eliminate the passband splitting [5]. As will be shown in subsequent sections, the cell modes of the fifth passband are hybrid modes resulting from the coupling of degenerate modes, such as TM_{030} and TM_{012}.

II. PERTURBATION THEORY FOR DEGENERATED MODES IN RF CAVITIES

Perturbation theory, typically used to analyze multicell SRF cavities, works well in cases where the resonance frequencies of the passband modes do not coincide [6]. However, in certain cavities, such as deflecting cavities [7] or traveling-wave cavities with a feedback waveguide [8], degenerate modes exist; for example, two dipole modes with different polarizations or partially orthogonal standing-wave (SW) modes forming the traveling wave. In this case, the linear perturbation theory does not apply, and a coupled-mode theory is used. Below is a brief outline of this approach to multicell SRF cavities based on the work [9], which details the effects of the mode interaction in rf cavities.

Consider a *concave* deformation of a cavity with two orthogonal modes, α and β, having close frequencies ω_α and ω_β. The fields of these modes are $\vec{H}_\alpha$ and $\vec{E}_\alpha$ and $\vec{H}_\beta$ and $\vec{E}_\beta$, respectively. These fields satisfy ideal boundary conditions on the unperturbed cavity surface S. Figure 3 illustrates a cavity with a small concave deformation. The unperturbed cavity has volume V, and the volume of perturbation is ΔV. The field of a deformed cavity may be expressed, to a first approximation, via the fields of an ideal cavity as:

$$\vec{H} \approx h_\alpha \vec{H}_\alpha + h_\beta \vec{H}_\beta, \tag{1}$$

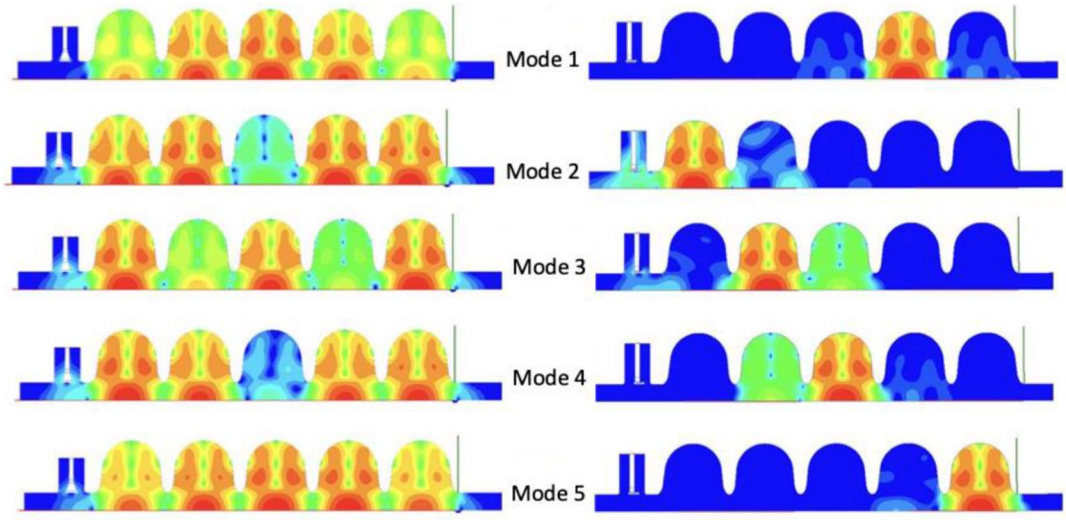


FIG. 2. Electric field maps for hybrid modes of the fifth monopole passband in the initial design of a five-cell 650 MHz SRF cavity with the $\beta_G = 0.9$ for the PIP-II project: for the cases of an ideal cavity (left) and a cavity with manufacturing tolerances of ± 0.2 mm rms (right).

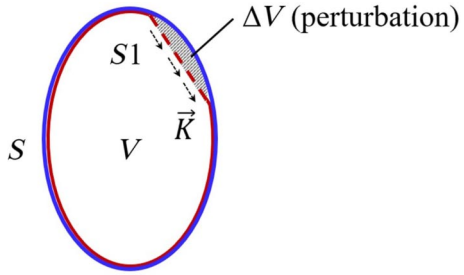


FIG. 3. Concept of a cavity of volume V with a small perturbation ΔV; the unperturbed and perturbed geometries are shown by blue and red lines, respectively, along with the surface currents $\vec{K}$ on the interface surface S_1.

$$\vec{E} \approx e_\alpha \vec{E}_\alpha + e_\beta \vec{E}_\beta, \tag{2}$$

with ideal boundary conditions on the deformed cavity surface S_1:

$$\vec{n} \times \vec{E} = 0, \tag{3}$$

$$\vec{n} \cdot \vec{H} = 0. \tag{4}$$

To eliminate the field in the perturbation volume ΔV, we introduce the *electric* currents $\vec{K}$ on the surface S_1, assuming that the tangential component of the electric field $\vec{E}$ on the S_1 is zero, in accordance with Eq. (3). In this case, the magnetic field amplitudes h_α and h_β of the modes are:

$$h_\alpha = \frac{\omega_\alpha \int_{S_1} \vec{K} \cdot \vec{E}_\alpha dS}{i(\omega^2 - \omega_\alpha^2)\mu_0 \int_V \vec{H}_\alpha \cdot \vec{H}_\alpha dV}, \tag{5}$$

$$h_\beta = \frac{\omega_\beta \int_{S_1} \vec{K} \cdot \vec{E}_\beta dS}{i(\omega^2 - \omega_\beta^2)\mu_0 \int_V \vec{H}_\beta \cdot \vec{H}_\beta dV}. \tag{6}$$

Here ω is the resonance frequency of the deformed cavity, $\omega \approx \omega_\alpha \approx \omega_\beta$.

On the other hand, according to Eq. (1), on S_1, we have

$$\vec{K} = -\vec{n} \times \vec{H} \approx -h_\alpha(\vec{n} \times \vec{H}_\alpha) - h_\beta(\vec{n} \times \vec{H}_\beta). \tag{7}$$

Substituting Eq. (7) into Eqs. (5) and (6), using Maxwell's equations and relevant vector theorems, we get dispersion equations, which determine resonance frequencies of the two-mode system and the normal modes [9]:

$$\omega_\alpha^2 h_\alpha \left[1 + \frac{\int_{\Delta V}(\mu_0|\vec{H}_\alpha|^2 - \varepsilon_0|\vec{E}_\alpha|^2)dV}{\mu_0 \int_V |\vec{H}_\alpha|^2 dV}\right] - \omega^2 h_\alpha + \omega_\alpha^2 h_\beta \frac{\int_{\Delta V}(\mu_0 \vec{H}_\alpha \cdot \vec{H}_\beta - \frac{\omega_\beta}{\omega_\alpha}\varepsilon_0 \vec{E}_\alpha \cdot \vec{E}_\beta)dV}{\mu_0 \int_V |\vec{H}_\alpha|^2 dV} = 0, \tag{8}$$

$$\omega_\beta^2 h_\beta \left[1 + \frac{\int_{\Delta V}(\mu_0|\vec{H}_\beta|^2 - \varepsilon_0|\vec{E}_\beta|^2)dV}{\mu_0 \int_V |\vec{H}_\beta|^2 dV}\right] - \omega^2 h_\beta + \omega_\beta^2 h_\alpha \frac{\int_{\Delta V}(\mu_0 \vec{H}_\beta \cdot \vec{H}_\alpha - \frac{\omega_\alpha}{\omega_\beta}\varepsilon_0 \vec{E}_\beta \cdot \vec{E}_\alpha)dV}{\mu_0 \int_V |\vec{H}_\beta|^2 dV} = 0. \tag{9}$$

Equations (8) and (9) may be rewritten the following way:

$$\begin{aligned} h_\alpha[\omega_\alpha^2(1 + z|\alpha\alpha) - \omega^2] + h_\beta \omega_\alpha^2 z_{\alpha\beta} &= 0, \\ h_\alpha \omega_\beta^2 z_{\beta\alpha} + h_\beta[\omega_\beta^2(1 + z|\beta\beta) - \omega^2] &= 0, \end{aligned} \tag{10}$$

where

$$\begin{aligned} z_{\alpha\alpha} &= \frac{\int_{\Delta V}(\mu_0|\vec{H}_\alpha|^2 - \varepsilon_0|\vec{E}_\alpha|^2)dV}{\mu_0 \int_V |\vec{H}_\alpha|^2 dV}, \\ z_{\beta\beta} &= \frac{\int_{\Delta V}(\mu_0|\vec{H}_\beta|^2 - \varepsilon_0|\vec{E}_\beta|^2)dV}{\mu_0 \int_V |\vec{H}_\beta|^2 dV}, \\ z_{\alpha\beta} &= \frac{\int_{\Delta V}(\mu_0 \vec{H}_\alpha \cdot \vec{H}_\beta - \frac{\omega_\beta}{\omega_\alpha}\varepsilon_0 \vec{E}_\alpha \cdot \vec{E}_\beta)dV}{\mu_0 \int_V |\vec{H}_\alpha|^2 dV}, \\ z_{\beta\alpha} &= \frac{\int_{\Delta V}(\mu_0 \vec{H}_\beta \cdot \vec{H}_\alpha - \frac{\omega_\alpha}{\omega_\beta}\varepsilon_0 \vec{E}_\beta \cdot \vec{E}_\alpha)dV}{\mu_0 \int_V |\vec{H}_\beta|^2 dV}. \end{aligned} \tag{11}$$

The system of linear Eq. (10) can be represented in the matrix form:

$$\begin{pmatrix} \omega_\alpha^2(1 + z_{\alpha\alpha}) - \omega^2 & \omega_\alpha^2 z_{\alpha\beta} \\ \omega_\beta^2 z_{\beta\alpha} & \omega_\beta^2(1 + z_{\beta\beta}) - \omega^2 \end{pmatrix} \begin{pmatrix} h_\alpha \\ h_\beta \end{pmatrix} = 0. \tag{10'}$$

The resonance frequencies correspond to zeros of the matrix determinant:

$$\begin{vmatrix} \omega_\alpha^2(1 + z_{\alpha\alpha}) - \omega^2 & \omega_\alpha^2 z_{\alpha\beta} \\ \omega_\beta^2 z_{\beta\alpha} & \omega_\beta^2(1 + z_{\beta\beta}) - \omega^2 \end{vmatrix} = 0. \tag{10''}$$

It is a secular equation for two coupled oscillators, e.g., see Ref. [10]. From this equation, it follows that the resonance frequencies are given by a well-known formula [9]:

$$\omega_{\pm}^2 = \frac{\omega_\alpha^2(1+z_{\alpha\alpha}) + \omega_\beta^2(1+z_{\beta\beta})}{2} \pm \pm \sqrt{\left[\frac{\omega_\alpha^2(1+z_{\alpha\alpha}) - \omega_\beta^2(1+z_{\beta\beta})}{2}\right]^2 + \omega_\alpha^2\omega_\beta^2 z_{\alpha\beta}z_{\beta\alpha}}. \tag{12}$$

The amplitudes of the normal modes are the eigenvectors of the problem (10):

$$h_\alpha[\omega_\alpha^2(1+z_{\alpha\alpha}) - \omega_{\pm}^2] + h_\beta\omega_\alpha^2 z_{\alpha\beta} = 0. \tag{13}$$

The parameter $Z = \sqrt{z_{\alpha\beta}z_{\beta\alpha}}$ characterizes the coupling between the modes. If the coupling parameter is nonzero but the difference between the mode frequencies is sufficiently large, such that:

$$\left|\frac{\omega_\alpha^2(1+z_{\alpha\alpha}) - \omega_\beta^2(1+z_{\beta\beta})}{2}\right| \gg \omega_\alpha\omega_\beta Z, \tag{14}$$

then the coupling between the modes is negligible, and the modes α and β can be treated as independent, with their respective fields $\vec{H}_\alpha$ and $\vec{E}_\alpha$ and $\vec{H}_\beta$ and $\vec{E}_\beta$. The corresponding mode frequencies are $\omega'_\alpha = \omega_\alpha\sqrt{1+z_{\alpha\alpha}} \approx \omega_\alpha(1+\frac{1}{2}z_{\alpha\alpha})$ and $\omega'_\beta \approx \omega_\beta(1+\frac{1}{2}z_{\beta\beta})$, where the approximations hold for small perturbations, i.e., $z_{\alpha\alpha}$ and $z_{\beta\beta} \ll 1$. These expressions are consistent with Slater's perturbation theorem. Criterion [Eq. (14)] can be rewritten in terms of the perturbed mode frequencies as:

$$|\omega'_\alpha - \omega'_\beta| \gg \frac{2\omega_\alpha\omega_\beta}{\omega'_\alpha + \omega'_\beta} Z. \tag{15}$$

Using the arithmetic–geometric mean inequality, we obtain for small perturbations the following stronger criterion:

$$|\omega'_\alpha - \omega'_\beta| / \sqrt{\omega'_\alpha\omega'_\beta} \gg Z. \tag{16}$$

III. MODE INTERACTION IN A PILLBOX CAVITY

To understand the phenomenon of mode interaction in a multicell periodic structure, we first consider an ideal multicell cavity composed of pillbox cells operating at the TM_{010} mode and separated by thin diaphragms. The cell geometry is characterized by a radius R and a length $d = \frac{\beta_G\lambda_{010}}{2}$, where β_G is the geometric beta of the periodic structure designed to accelerate particles with a velocity $\beta = v/c = \beta_G$. Pillbox cells are coupled via beam apertures of radius a in the diaphragms. Let us first consider a separate cell. The higher-order modes TM_{012} and TM_{020} in a pillbox cell have the following resonant frequencies:

$$\omega_{012} = c\sqrt{\left(\frac{\nu_{01}}{R}\right)^2 + \left(\frac{\pi}{d}\right)^2}, \qquad \omega_{020} = c\frac{\nu_{02}}{R}. \tag{17}$$

This pair of modes is degenerate at $\beta_G = 0.968$, i.e., $\omega_{012} = \omega_{020} = \omega_0$. Let us model the beam apertures as axisymmetric protrusions on the end walls, each with a volume of $\Delta V/2$, and consider the mode mixing caused by these apertures. Note that in this case, we have *convex* deformations, and therefore, the quantity ΔV should be taken *with the negative sign.* To prove this, one may use the same technique as in Ref. [9] but introduce *magnetic* currents $\vec{N}$ on the inner surface of the perturbation volume ΔV. Since the aperture radius a is small compared to the wavelength $\lambda_{012} = \lambda_{020}$, by setting $\vec{H}_\alpha = \vec{H}_{012}$ and $\vec{H}_\beta = \vec{H}_{020}$, one can use Eq. (1) for the total field.

For the partial modes under consideration:

$$\begin{aligned} E_{\alpha z} &= E_\alpha \cos\left(\frac{2\pi z}{d}\right) J_0\left(\frac{\nu_{01} r}{R}\right), \\ E_{\alpha r} &= E_\alpha \frac{2\pi R}{\nu_{01} d} \sin\left(\frac{2\pi z}{d}\right) J_1\left(\frac{\nu_{01} r}{R}\right), \\ H_{\alpha\varphi} &= i\frac{E_\alpha}{Z_0}\frac{\nu_{02}}{\nu_{01}} \cos\left(\frac{2\pi z}{d}\right) J_1\left(\frac{\nu_{01} r}{R}\right), \end{aligned} \tag{18}$$

and

$$\begin{aligned} E_{\beta z} &= E_\beta J_0\left(\frac{\nu_{02} r}{R}\right), \\ E_{\beta r} &= 0, \\ H_{\beta\varphi} &= i\frac{E_\beta}{Z_0} J_1\left(\frac{\nu_{02} r}{R}\right). \end{aligned} \tag{19}$$

From Eq. (13), one has

$$h_\alpha[\omega_0^2(1+Z_{\alpha\alpha}) - \omega_{\pm}^2] + h_\beta\omega_0^2 Z_{\alpha\beta} = 0,$$

and therefore,

$$h_\beta = -h_\alpha \frac{\omega_0^2(1+Z_{\alpha\alpha}) - \omega_{\pm}^2}{\omega_0^2 Z_{\alpha\beta}}. \tag{20}$$

Here,

$$Z_{pq} \approx \frac{\int_{\Delta V}(\mu_0\vec{H}_p\cdot\vec{H}_q - \varepsilon_0\vec{E}_p\cdot\vec{E}_q)dV}{\mu_0\int_V |\vec{H}_p|^2 dV}, \tag{21}$$

where p and q take the values α and β. For a small protrusion near the axis, a direct calculation using Eqs. (11), (18), and (16) and neglecting the magnetic field yields

$$
\begin{aligned}
Z_{\alpha\alpha} &\approx 2\frac{\Delta V}{V}\left(\frac{\nu_{01}}{\nu_{02}}\right)^2\frac{1}{J_1^2(\nu_{01})},\\
Z_{\beta\beta} &\approx \frac{\Delta V}{V}\frac{1}{J_1^2(\nu_{02})},\\
Z_{\alpha\beta} &\approx 2\frac{\Delta V}{V}\left(\frac{\nu_{01}}{\nu_{02}}\right)^2\frac{1}{J_1^2(\nu_{01})}\frac{E_\beta}{E_\alpha} = Z_{\alpha\alpha}\frac{E_\beta}{E_\alpha},\\
Z_{\beta\alpha} &\approx \frac{\Delta V}{V}\frac{1}{J_1^2(\nu_{02})}\frac{E_\alpha}{E_\beta} = Z_{\beta\beta}\frac{E_\alpha}{E_\beta}.
\end{aligned}
\tag{22}
$$

Note that we have taken into account that the perturbation is *convex*, which gives the positive sign of the quantity Z_{pq} (see above).

From Eqs. (12) and (22), one has

$$
\omega_\pm^2 = \omega_0^2\left(1+\frac{Z_{\alpha\alpha}+Z_{\beta\beta}}{2}\pm\frac{Z_{\alpha\alpha}+Z_{\beta\beta}}{2}\right). \tag{23}
$$

As follows from Eqs. (18) and (19), the magnetic fields of the eigenmodes at radii $r < a$ are equal to:

$$
\begin{aligned}
H_{\alpha\varphi} &\approx i\frac{E_\alpha}{2Z_0}\frac{\nu_{02}r}{R}\cos\left(\frac{2\pi z}{d}\right),\\
H_{\beta\varphi} &\approx i\frac{E_\beta}{2Z_0}\frac{\nu_{02}r}{R}.
\end{aligned}
\tag{24}
$$

In this case, the total azimuthal magnetic field has the following form, taking into account Eq. (1):

$$
H_\varphi(r,z)\approx i\frac{h_\alpha E_\alpha}{2Z_0}\frac{\nu_{02}r}{R}\left\{\cos\left(\frac{2\pi z}{d}\right)+\frac{1}{2}[(\eta-1)\pm(\eta+1)]\right\}, \tag{25}
$$

here

$$
\eta = \frac{1}{2}\left(\frac{\nu_{02}J_1(\nu_{01})}{\nu_{01}J_1(\nu_{02})}\right)^2 = 6.11.
$$

As follows directly from Maxwell's equation curl $\vec{H} = i\omega_0\varepsilon_0\vec{E}$, the total longitudinal electric field on axis is

$$
E_z(r,z)\approx h_\alpha E_\alpha\left\{\cos\left(\frac{2\pi z}{d}\right)+\frac{1}{2}[(\eta-1)\pm(\eta+1)]\right\}.
$$

Let us examine these two modes in more detail.

a) For the "+" mode:

$$
\begin{aligned}
\omega_+^2 &= \omega_0^2(1+Z_{\alpha\alpha}+Z_{\beta\beta})\\
&= \omega_0^2\left[1+\frac{\Delta V}{V}\left(\left(\frac{\nu_{01}}{\nu_{02}}\right)^2\frac{2}{J_1^2(\nu_{01})}+\frac{1}{J_1^2(\nu_{02})}\right)\right],
\end{aligned}
$$

and the fields near the axis are

$$
\begin{aligned}
E_z(r,z) &\approx h_\alpha E_\alpha\left[\cos\left(\frac{2\pi z}{d}\right)+\eta\right],\\
H_\varphi(r,z) &\approx i\frac{h_\alpha E_\alpha}{2Z_0}\frac{\nu_{02}r}{R}\left[\cos\left(\frac{2\pi z}{d}\right)+\eta\right].
\end{aligned}
\tag{26}
$$

b) For the "−" mode:

$$
\omega_-^2 = \omega_0^2,
$$

and the fields near the axis are

$$
\begin{aligned}
E_z(r,z) &\approx h_\alpha E_\alpha\left[\cos\left(\frac{2\pi z}{d}\right)-1\right],\\
H_\varphi(r,z) &\approx i\frac{h_\alpha E_\alpha}{2Z_0}\frac{\nu_{02}r}{R}\left[\cos\left(\frac{2\pi z}{d}\right)-1\right].
\end{aligned}
\tag{27}
$$

On the cavity walls, i.e., at $z = 0$ or $z = d$, both electric and magnetic fields are zero. Thus, the distribution of the fields in the cavity is independent of the boundary conditions on the protrusion. This means that the cavity cannot be excited through apertures on the axis, and this is also a manifestation of the well-known resonance disappearance effect discovered for degenerate dipole modes [9,11]. Figure 4 illustrates the effect of mode mixing for the degenerate modes discussed above, while Fig. 5 shows the normalized longitudinal component of the electric field on axis for the − mode. The blue curve in Fig. 5 is calculated numerically for a pillbox cavity with protrusions (see Fig. 4, right plots), and the red one is calculated analytically using Eq. (27).

Mode mixing, which leads to the vanishing of the electromagnetic field near the coupling apertures, can also be observed for other pairs of modes; see Fig. 6, which shows the calculated HOM frequencies of a pillbox cavity. The red dots correspond to the degeneracy between the TM_{0n0} and TM_{0m2} modes, which results in zero electromagnetic fields on the axis near the cavity end walls.

For example, for the TM_{030} and TM_{022} modes, degeneracy occurs at $\beta_G = d/(\lambda_{010}/2) = 0.72168$. Consequently, if the TM_{0n0} and TM_{0m2} modes are degenerate, it is easy to see from Eqs. (17)–(27) that, in the first approximation, the electromagnetic field near the axis next to the cavity end walls is zero.

Consider a multicell cavity comprised of pillbox cells coupled via apertures. For degenerate modes, both magnetic and electric fields on the axis near the end walls are small. In this case, the intercell coupling coefficient is $K_c \ll 1$. Here the intercell coupling coefficient is determined as $K_c = 2\frac{\omega_\pi-\omega_0}{\omega_\pi+\omega_0}$; ω_π and ω_0 are the resonance frequencies of the modes π and 0, respectively. Figure 7 illustrates the behavior of the coupling coefficient K_c for

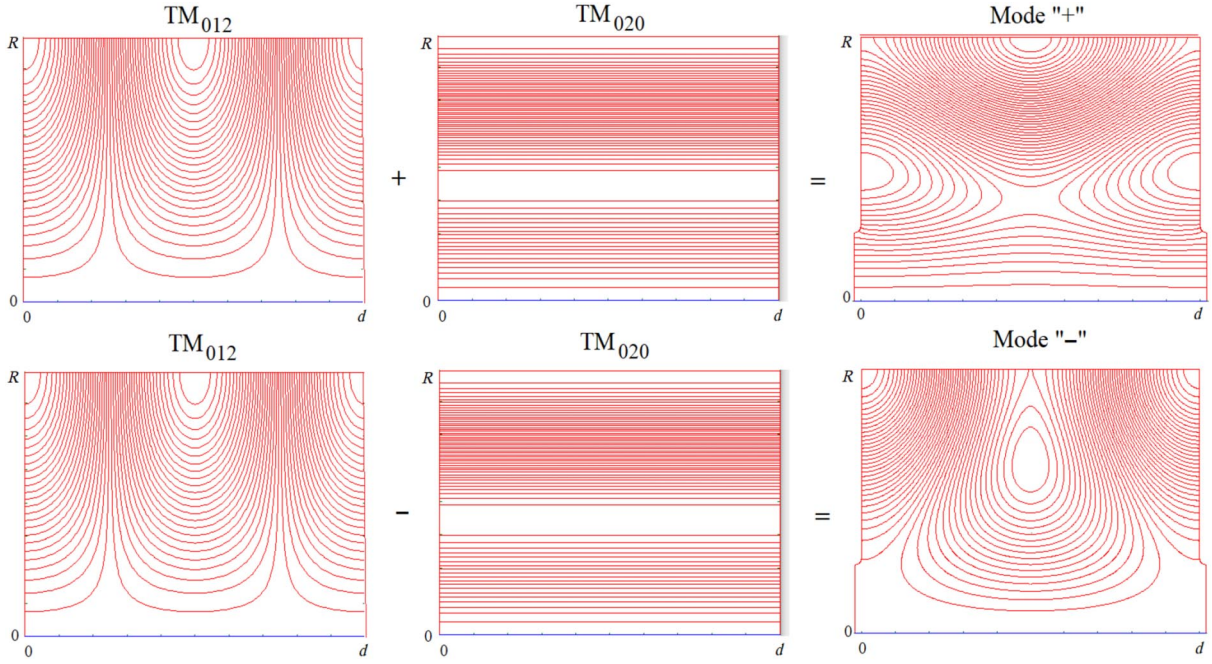


FIG. 4. Mode interaction in a pillbox cavity. Left and center plots: electric field maps of the unperturbed partial modes TM_{012} and TM_{020}. Right plots: hybrid + mode (top plot) and − mode (bottom plot) in the presence of protrusions on the cavity end walls.

two hybrid modes, + and −, of such a periodic structure as a function of the normalized coupling aperture radius a/R. One can see that the coupling for the mode − is very weak up to $a/R \approx 0.45$, whereas the coupling for the mode + increases with the aperture as a^3 [12] up to $a/R \approx 0.3$. Since the hybrid mode $-$ K_c is very small, the frequencies of the multicell cavity in this passband are practically independent of the phase shift per cell. This implies that the passband is "flat." However, with a flat passband, the field distribution for the normal SW HOM along the multicell cavity becomes highly sensitive to perturbations in cell frequencies.

According to Ref. [6], the relative field perturbation $\frac{\delta X}{X}$ of the SW mode in a multicell cavity is proportional to the perturbation of the cell frequency $\delta\omega$ over the intercell coupling K_c:

$$\frac{\delta X}{X} \frac{\tilde{1}}{K_c} \frac{\delta\omega}{\omega}.$$

Here X is the amplitude of a normal mode in a multicell cavity, and δX is its perturbation caused by manufacturing errors; ω is the resonance frequency of this normal mode.

It should be noted that, during the cavity tuning process, field flatness is achieved only for the operating mode. For HOMs, the cell resonance frequencies may differ, resulting in a significant $\frac{\delta\omega}{\omega}$. For a very small K_c (flat bandwidth), it is easy to obtain $\frac{\delta X}{X} \gtrsim 1$, and consequently, these are no longer conventional standing-wave modes in a multicell cavity, but rather individual cell resonances. This is exactly what was observed for the HB650 cavities; see Figs. 1 and 2.

Therefore, this simple model allows us to draw the following important conclusions regarding a multicell cavity composed of pillbox cells coupled via the beam apertures on the cavity axis: (i) If the modes TM_{0n0} and TM_{0m2} are degenerate, they form two normal modes with different frequencies and different field distributions. (ii) One of the normal modes has very small electric and magnetic fields near the coupling aperture, where the partial modes compensate each other. This, in turn. leads to very weak coupling between the cells, i.e., a flat dispersion curve. Such a flat passband in a multicell cavity results in individual cell resonances rather than classical SW modes, and, at the same time, such a structure can exhibit large R/Q and a highly loaded quality factor. (iii) To first approximation, this compensation does not depend on the aperture radius a, and for a fixed cell length, one could

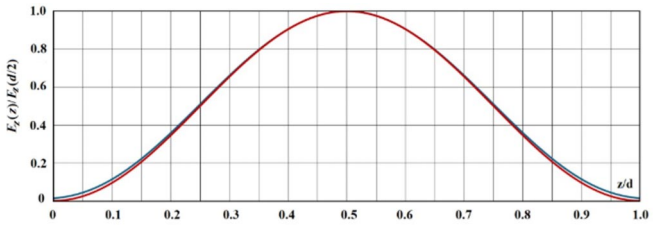


FIG. 5. Axial distribution of the longitudinal electric field in a pillbox cavity. Blue curve: numerical simulation results for a pillbox cavity with protrusions. Red curve: analytical calculations using Eq. (27).

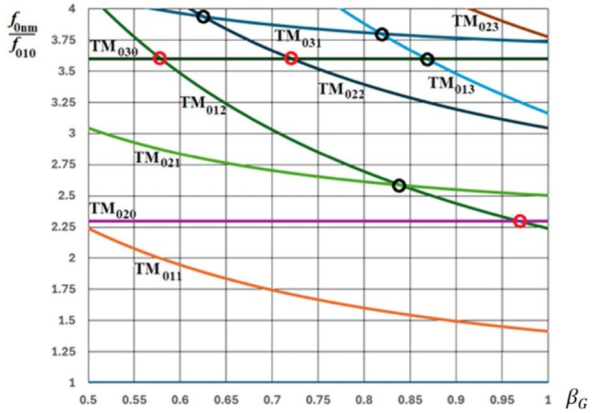


FIG. 6. Normalized frequencies of the HOMs in a pillbox cavity as a function of parameter $\beta_G = d/(\lambda_{010}/2)$, where d is the cavity length and λ_{010} is the wavelength of the operating TM_{010} mode.

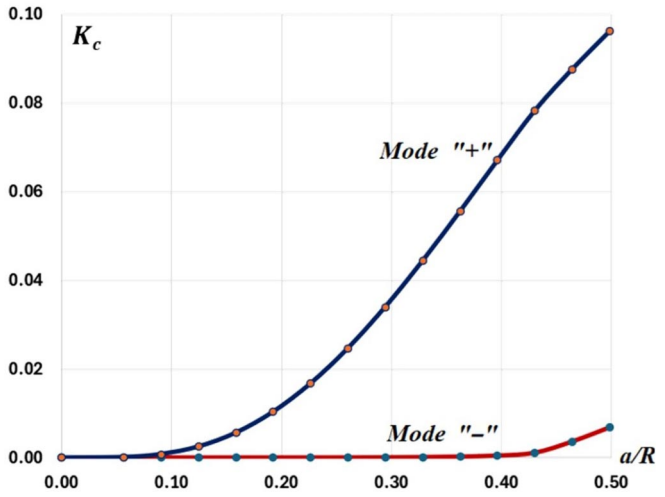


FIG. 7. Coupling coefficient K_c for the normal modes corresponding to the coupled TM_{020} and TM_{012} modes in a multicell pillbox cavity as a function of the normalized aperture radius.

simply use an enlarged beam aperture to increase the intercell coupling. However, this approach may prove impractical, as it leads to an increase in the electric field enhancement factor in real cavities. (iv) To reduce mode interaction, mode degeneracy should be eliminated and the partial modes detuned. According to Eq. (16), the relative frequency difference must exceed the coupling between the modes, i.e.,

$$|\omega'_\alpha - \omega'_\beta|/\sqrt{\omega'_\alpha \omega'_\beta} \gg \sqrt{z_{\alpha\beta} z_{\beta\alpha}}.$$

One way to mitigate this effect is to use a different cell length, or β_G, if permitted by the beam dynamics.

IV. MODE INTERACTION IN AN ELLIPTICAL SRF CAVITY

Let us consider an axisymmetric elliptical cavity, making the following general assumptions: (i) The cavity cells are symmetric left-to-right. (ii) There are two degenerate *axisymmetric* modes with an even variation in the longitudinal direction, namely, TM_{0n0} and TM_{0m2}. (iii) The cells have equal apertures, which are small compared to the wavelengths $\lambda_{0n0} = \lambda_{0m2}$.

The elliptical cell model is shown in Fig. 8. The ideal cell with volume V has no coupling apertures, and its inner surface S is outlined in black. The coupling slots are treated as a perturbation. They have surface S_1 outlined in blue and volume ΔV (shaded areas). Taking $\vec{H}_\alpha = \vec{H}_{0m2}$ and $\vec{H}_\beta = \vec{H}_{0n0}$, we can use Eq. (1) for the total field.

Because both partial modes are axisymmetric, near the axis, the components $E_{\alpha z}$ and $E_{\beta z}$ are independent of the radius r in the first approximation. At the cavity ends, i.e., for $z = 0$ and $z = d$, see Fig. 8, one has $E_{\alpha z} \approx E_{\alpha 0}$ and $E_{\beta z} \approx E_{\beta 0}$ for $r \ll \lambda_{0m2} = \lambda_{0n0}$. The magnetic field there is weak and can be neglected. Due to mode degeneracy $\omega_\alpha = \omega_\beta = \omega_0$, and in this case, the quantities z_{pq} can be estimated as follows, neglecting the magnetic field:

$$\begin{aligned} z_{\alpha\alpha} &= \frac{\varepsilon_0 E_{\alpha 0}^2 \Delta V}{\mu_0 \int_V |\vec{H}_\alpha|^2 dV}, \\ z_{\beta\beta} &= \frac{\varepsilon_0 E_{\beta 0}^2 \Delta V}{\mu_0 \int_V |\vec{H}_\beta|^2 dV}, \\ z_{\alpha\beta} &= \frac{\varepsilon_0 E_{\alpha 0} E_{\beta 0} \Delta V}{\mu_0 \int_V |\vec{H}_\alpha|^2 dV}, \\ z_{\beta\alpha} &= \frac{\varepsilon_0 E_{\beta 0} E_{\alpha 0} \Delta V}{\mu_0 \int_V |\vec{H}_\beta|^2 dV}. \end{aligned} \tag{28}$$

Note that we again take into account that the perturbation is *convex;* see previous section. From Eq. (28), it follows that:

$$z_{\alpha\alpha} z_{\beta\beta} = z_{\alpha\beta} z_{\beta\alpha}. \tag{29}$$

From Eqs. (12) and (29), one has the same expression for frequencies of the normal modes as for the pillbox cell; see Eq. (23):

$$\omega_\pm^2 = \omega_0^2 \left(1 + \frac{Z_{\alpha\alpha} + Z_{\beta\beta}}{2} \pm \frac{Z_{\alpha\alpha} + Z_{\beta\beta}}{2}\right). \tag{30}$$

Here, for the mode −, the resonant frequency is equal to ω_0 and, therefore, according to Eqs. (13) and (28)

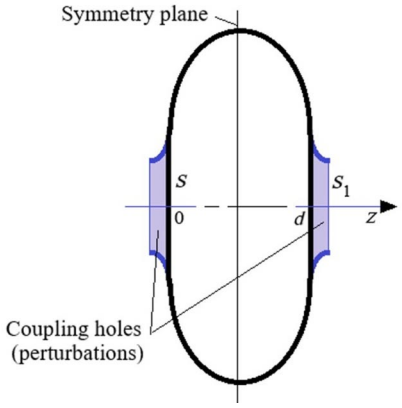


FIG. 8. The cell geometry of an axisymmetric elliptical SRF cavity. The cell has left-to-right symmetry.

$$h_\beta = -h_\alpha \frac{z_{\alpha\alpha}}{z_{\alpha\beta}} = -h_\alpha \frac{E_{\alpha 0}}{E_{\beta 0}}. \tag{31}$$

The azimuthal component of the magnetic field of the eigenmodes α and β next to the axis at $z = 0$ and $z = d$ can be found using Maxwell's equation $\operatorname{curl} \vec{H}_{\alpha,\beta} = -i\omega_0 \varepsilon_0 \vec{E}_{\alpha,\beta}$:

$$H_{\alpha,\beta,\varphi}(r) = -i\frac{r}{2}\omega_0 \varepsilon_0 E_{\alpha,\beta 0}. \tag{32}$$

And, thus, according to Eq. (31), the resulting field for $z = 0$ and $z = d$ of the normal mode $-$ is equal to:

$$H_\varphi(r) = -i\frac{r}{2}\omega_0 \varepsilon_0 (h_\alpha E_{\alpha 0} + h_\beta E_{\beta 0}) = 0. \tag{33}$$

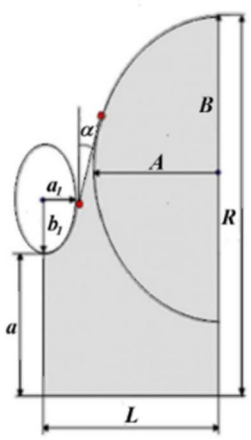
From Maxwell's equation $\operatorname{curl} \vec{H} = -i\omega_0 \varepsilon_0 \vec{E}$ and Eq. (33), it follows that for the $-$ mode at $z = 0$ and $z = d$:

$$E_z(r) = 0.$$

The radial component of the electric field of the mode $-$ is also equal to zero, because the partial eigenmodes $\vec{E}_\alpha$ and $\vec{E}_\beta$ have no radial components at the ends of the ideal cell, i.e., at $z = 0$ and $z = d$.

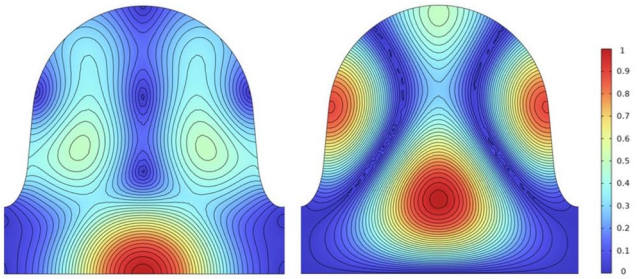
This means that, near the coupling aperture, all electromagnetic field components of the mode $-$ are equal to zero, just as was the case for pillbox cells. Consequently, all the conclusions formulated in the previous section are also valid for elliptical cavities.

Figure 9 shows the geometric parameters of the elliptical cell (a) and electric and magnetic field maps (b) for the hybrid modes of the fifth monopole passband of the $\beta_G = 0.9$, 650 MHz SRF cavity for the PIP-II linac [4]. The hybrid cavity mode at 1988 MHz results from the mixing of a pair of degenerate TM_{030} and TM_{012} cell modes. One can see that, in the hybrid mode, the electric and magnetic fields near the coupling aperture are zero, and therefore, there is no coupling between the cells,

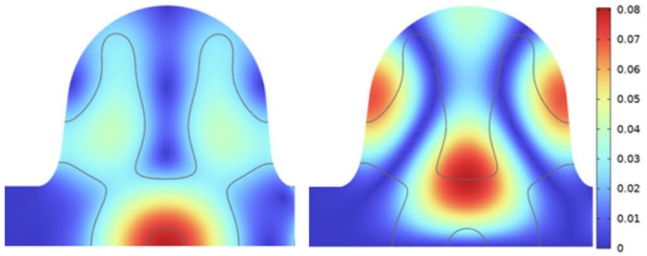


Dimension	Regular cell	End cell
a, mm	50	50
R, mm	200.3	200.3
L, mm	103.8	107.0
A, mm	82.5	82.5
B, mm	84	84.5
a_1, mm	18	20
b_1, mm	38	39.5
α, deg	5.2	7

(a)



(b)



(c)

FIG. 9. (a) Geometric parameters of the elliptical cells for the initial PIP-II high-beta cavity design (650 MHz, $\beta_G = 0.9$). (b) Electric field distribution (left) and magnetic field distribution (right) illustrate mode mixing in the inner cell of this cavity. (c) Electric field distribution (left) and magnetic field distribution (right) in the end cells (courtesy of I. Gonin).

which creates the trapped modes. At the same time, the cavity shape is optimized to achieve acceptable peak surface fields and low surface losses for the operating mode.

However, as shown in Figs. 2 and 9, the end half-cells differ in size from the regular half-cells, indicating that the end cells lack longitudinal symmetry. In addition, each end half-cell is terminated by the beam pipe. Nevertheless, the

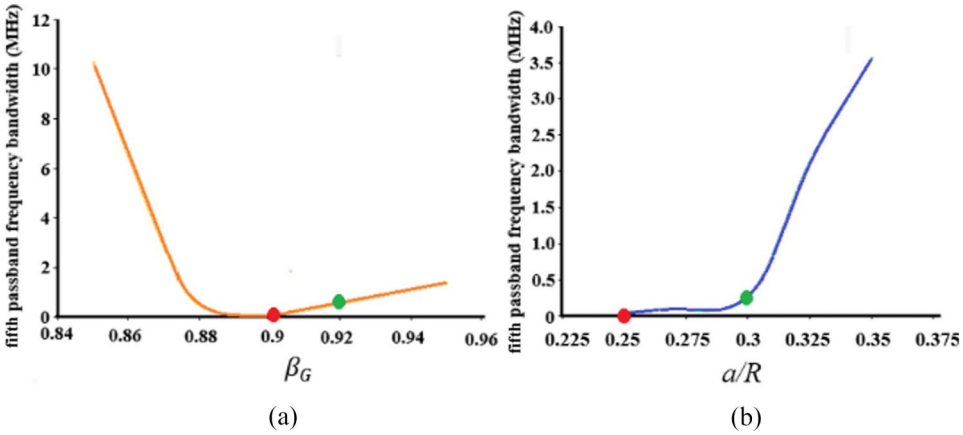


FIG. 10. Dependence of the fifth monopole passband bandwidth on the geometric beta, β_G (a) and the normalized beam aperture (b). The red dots correspond to the initial cavity with $\beta_G = 0.9$ and an aperture radius of 50 mm. The green dots correspond to alternative cavity designs with $\beta_G = 0.92$ and an aperture radius of 50 mm (a) and with $\beta_G = 0.9$ and an aperture radius of 60 mm (b).

field amplitudes remain small near the end-cell irises, as shown in Fig. 9(c), because the perturbation is determined primarily by the beam holes, as indicated by the cell geometric parameters shown in Fig. 9(a). Therefore,

$$z_{\alpha\alpha} z_{\beta\beta} \approx z_{\alpha\beta} z_{\beta\alpha},$$

because $\Delta V_{\text{holes}} \gg \Delta V_{\text{walls}}$. The rms manufacturing and processing errors are typically even smaller; see Ref. [13]. However, in each case, a thorough numerical analysis that accounts for misalignments is necessary to ensure that no HOM interactions occur, which might lead to weak intercell coupling.

The frequency bandwidth $\Delta f = K_c f_0$ (f_0 is the passband average frequency) of the fifth monopole passband versus β_G and the ratio of the aperture a over the cavity equatorial radius R is shown in Fig. 10 [4]. Note that the cell parameters were reoptimized for various values of β_G and a/R. Nevertheless, the dependence of the bandwidth on the cavity aperture exhibits the same trend as for the pillbox case shown in Fig. 6: for the a/R ratio of less than 0.3 (or an aperture smaller than ~60 mm), the bandwidth is very small, but it increases rapidly for the larger apertures. One can see that increasing β_G to 0.92 provides a bandwidth exceeding 0.5 MHz, which is sufficient to eliminate mode splitting into individual cell resonances, as well as to achieve an acceptable R/Q and a low external quality factor Q_{ext}. The present design of the cavity for the high-energy section of the PIP-II linac features an increased beam aperture radius of 60 mm and $\beta_G = 0.92$. This configuration mitigates mode interaction [5] and ensures sufficient coupling for all modes of the fifth monopole passband to the input power coupler, thereby resulting in low external quality factors Q_{ext} of 10^5–10^6 range. The cavity shape has been reoptimized to keep the peak surface fields at the levels specified in the initial design. Using the predicted spread of the monopole HOM parameters: resonance frequencies, R/Q and Q_{ext}, one can generate many random linac configurations (typically about 10^5–10^6) to estimate the probability of

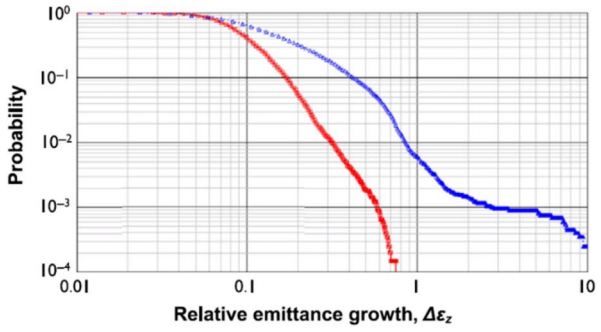


FIG. 11. Probability of longitudinal emittance growth in the high-energy 650 MHz part of the PIP-II linac. Data for the initial design of the cavity is shown in blue; data for the present design is in red.

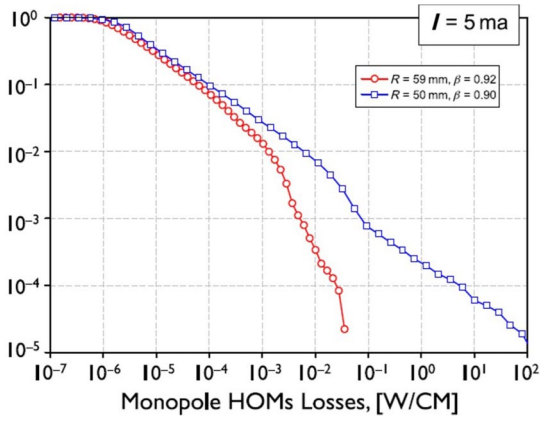


FIG. 12. Probability of monopole HOM rf losses per cryomodule for the initial (blue) and present (red) version of the PIP-II 650 MHz cavities. The beam current is 5 mA.

longitudinal emittance growth and rf losses per cryomodule.

Figure 11 shows the accumulated probability of longitudinal emittance growth in the high-energy section of the PIP-II linac at an average beam current of 5 mA.

Although the probability of significant emittance increase for the initial cavity design is low, $< 10^{-2}$, it could nevertheless limit the beam current for a future upgrade of the facility. The present design, however, does not pose problems regarding beam longitudinal emittance. The cumulative probability of HOM losses per cryomodule is presented in Fig. 12. One can see that the risk of high cryogenic losses is also significantly smaller for the present cavity design with $\beta_G = 0.92$.

V. CONCLUSIONS

The paper describes the effect of high-order mode interaction in a multicell SRF accelerating structure. In the case of degenerate monopole modes, the interaction results in splitting into two hybrid modes. One of these modes exhibits very weak electric and magnetic fields near the beam apertures. Consequently, the cells are effectively uncoupled for this mode, yielding a nearly flat passband.

The spread of HOM frequencies due to mechanical imperfections results in the flat passband being split into a set of localized cell resonances that are not coupled to the beam pipe, the fundamental power coupler, or the HOM couplers. These local resonances are characterized by large shunt impedance values and may induce undesirable effects, such as beam emittance dilution and increased cryogenic losses, thus limiting the beam current. This is particularly important for the future high-current SRF linacs such as those being developed for ADS projects [14,15]. Therefore, this phenomenon should be carefully considered during the design and optimization of the accelerating SRF cavities.

An analytical theory based on a mode-interaction model is developed to explain this effect. Possible mitigation strategies are also discussed. It is shown that the most effective approach is to modify the cell length (i.e., the geometric beta), provided that the beam dynamics requirements permit such a change.

It is worth noting that the mode-interaction effect is deliberately exploited in the rf windows of high-power couplers to minimize both the electric and magnetic fields in the ceramic-to-metal brazing region. An example is given in Ref. [16], where the interaction between the modes TE_{01} and TE_{02} is described.

ACKNOWLEDGMENTS

This work was supported by the U.S. Department of Energy, Office of Science. This manuscript has been authored by Fermi Forward Discovery Group, LLC under Contract No. DE-AC02-07CH11359 with the U.S. Department of Energy.

DATA AVAILABILITY

There are no publicly available research data or software supporting this manuscript. Requests for further information or data should be sent to the authors.

[1] J. Sekutowicz, HOM damping and power extraction from superconducting cavities, in *Proc. 2006 Linear Accel. Conf.* (Knoxville, TN, USA, 2006), pp. 506–510.

[2] I. V. Gonin, E. Borissov, A. Grassellino, C. J. Grimm, V. Jain, S. Kazakov, V. A. Lebedev, A. Lunin, C. S. Mishra, D. V. Mitchell, T. H. Nicol, Y. M. Pischalnikov, G. V. Romanov, A. M. Rowe, N. K. Sharma, N. Solyak, and V. P. Yakovlev, 650 MHz Elliptical Superconducting RF cavities for PIP-II project, in *Proc. 28th Int. Linear Accel. Conf.* (Lancing, MI, USA, 2016), pp. 943–945.

[3] N. Solyak, E. Gianfelice-Wendt, I. Gonin, S. Kazakov, V. A. Lebedev, S. Nagaitsev, J.-F. Ostiguy, N. Perunov, G. V. Romanov, and V. P. Yakovlev, The concept design of the CW linac of the Project X, in *Proc. Int. Part. Accel. Conf.* (Kyoto, Japan, 2010), pp. 654–656.

[4] A. Lunin, A. Saini, A. Sukhanov, N. Solyak, and V. Yakovlev, Alternative cavity for high energy part of the Project X linac, in *Proc. 2nd Int. Part. Accel. Conf.* (New Orlean, LA, USA, 2012), pp. 2997–2999.

[5] A. Lunin, T. Khabiboulline, N. Solyak, A. Sukhanov, and V. Yakovlev, Statistical analysis of the eigenmode spectrum in the SRF cavities with mechanical imperfections, *Proc. 13th Int. Comput. Accel. Phys. Conf. ICAP2018* (Key West, Florida, USA, 2018), p. 265.

[6] D. E. Nagle, E. A. Knapp, and B. C. Knapp, Coupled resonator model for standing wave accelerator tanks, Rev. Sci. Instrum. **38**, 1583 (1967).

[7] A. Citron, G. Dammertz, M. Grundner, L. Husson, R. Lehm, and H. Lengeler, The Karlsruhe–CERN superconducting RF separator, Nucl. Instrum. Methods Phys. Res. **164**, 31 (1979).

[8] R. B. R. Shersby-Harvi and L. B. Mullett, A travelling wave linear accelerator with R.F. power feedback, and an observation of R.F. absorption by gas in presence of a magnetic field, Proc. Phys. Soc. B **62**, 270 (1949).

[9] B. V. Schteinshleiger, *Phenomena of wave interactions in electromagnetic resonators* (Oborongiz, Moscow, Russian, 1955).

[10] L. D. Landau and E. M. Lifshits, *Quantum Mechanics* (Pergamon Press, New York, pp. 1965), p. 133.

[11] B. V. Schteinshleiger, Phenomena in electromagnetic resonators near the points of coincidence of resonance frequencies, Sov. Phys. Doklady **LXV**, 669 (1949).

[12] H. A. Bethe, Physics of diffraction by small holes, Phys. Rev. **66**, 163 (1944).

[13] A. Sulimov, G. Kreps, and J. Sekutowicz, Estimation of small geometry deviation for TESLA-shape cavities due to inner surface polishing, in *Proc. 16th Int. Conf. RF Supercond.* (Paris, France, 2013), pp. 537–539.

[14] R. Johnson and Ch Ankenbrandt, High power SRF linacs for ADS reactors, in *Proc. Int. Part. Accel. Conf.* (Kyoto, Japan, 2010), pp. 163–165.

[15] B. Yee-Rendon, Overview of ADS projects in the world, in *Proc. 31st Int. Linear Accel. Conf.* (Liverpool, UK, 2022), pp. 310–313.

[16] S. Kazakov, A new traveling-wave mixed-mode RF window with a low electric field in ceramic-metal brazing area, KEK preprint 98–140 (1998).